# Observation of Néel Skyrmions in an Exchange Coupled Cobalt/Palladium Based Multi-layers of Metallic Compounds at High Temperatures

B.U.V. Prashanth[1*] and Mohammed Riyaz Ahmed[2]

[1] School of Electronics and Communication Engineering, REVA University, Bengaluru, India
[2] School of Multidisciplinary Studies, REVA University, Bengaluru, India
[*] Corresponding author. E-mail: prashanthbuv@reva.edu.in

Received: July 19, 2020; Accepted: Oct. 05, 2020

In the class of cubic B20 transition metal silicides and germanides, the skyrmions and skyrmion lattices have so far been studied most extensively. Certain groups of materials in which skyrmions were identified include the Perovskites and Heusler systems. In this paper, the skyrmions chiral Néel characterization is illustrated via Lorentz transmission electron microscopy. Further utilizing magnetic-imaging and Hall-transport in a functionally viable multilayer sample, the topological-hall resistivity rises over a wide range of temperature and magnetic field with the isolated-skyrmion density is observed, verifying the effect of the skyrmion geometric-phase on electron transport. The observed bulk Néel skyrmions in an exchange coupled cobalt/palladium(Co/Pd) based multi-layers of metallic compounds at high temperatures up to a maximum of 220 K followed by a larger region characterized by spin from in-to out-of-plane. In fact, the skyrmions are extremely resilient to in-plane magnetic fields and can be stable in a zero magnetic field using appropriate cooling methods in field over a very wide ambient temperature of up to 5.5 K. At low temperatures (of < 13 K) the Néel skyrmions have been observed recently in distinct non-metallic compounds, in bulk crystals with broken inversion symmetry with a non-adiabatic footprint, multiband transport, interfacial interactions.

**Keywords:** Spintronics, Lorentz transmission electron microscopy, Magnetic Skyrmions, non-centrosymmetric, Dzyaloshinskii–Moriya interaction.

http://dx.doi.org/10.6180/jase.202104_24(2).0005

## 1. Introduction

The thin films interacting with a substrate comprehensively form spontaneous non-trivial spin textures that are illuminated by chiral spin interactions. The wide dimensionality of skyrmions in hetero-structures has considerable potential for use, and needs further conceptual and empirical study [1–3]. A direct minimum of three-dimensional (3D) in the standard energy function elucidates that cubic helimagnets chiral skyrmions are amplified along three spatial axes(in-to out-of-plane) in the thin films [4]. Chiral skyrmions are spintronics candidates of high mobility nanoscale spots of inverse magnetization and could be used in the emerging spin electronics. The cross-section of such 3D skyrmions can be thought of as an overlap of conical amplifications in the direction of skyrmion axis and spin is twisted twice in the vertical axis [5]. Numerical responses for chiral amplifications illustrate that transversally distorted helices based 3D skyrmion lattices are thermodynamically stable in a wide range of applied magnetic fields [6]. The Dzyaloshinskii–Moriya interaction (DMI) emerging in magnets of non-centrosymmetric nature, induce long-range amplifications with a fixed spin in magnetization. The DMI provides unique mechanism to stabilize chiral skyrmions and hopfions as 2D and 3D localized states [7]. The experimentally observed skyrmions and other chiral amplifications are in tandem with theory based results on the classical DMI model. The theoretical analysis elucidate that induced uniaxial anisotropy stabilizes skyrmions and

transversally distorted helices in ultra thin segments of cubic helimagnets [8]. In bulk cubic helimagnets, these chiral amplifications are present as meta-stable states. Recent experiments in FeGe and MnSi state that skyrmions are stabilized by an induced uniaxial anisotropy [9]. The exact magnetic structures of skyrmions emerging in confined cubic helimagnets are still to be explored. The heavy metal under-layer combined with spin-Hall physics allows the local magnetic state to be controlled easily [10]. The strong interfacial spin – orbit interaction occurs in a massive DMI interface, represented by the DMI constant, D. The DMI is a spin–orbit coupling (SoC) effect that emerges in broken inversion symmetry crystals. In these materials the combination of the SoC interactions and exchange energy between electrons paves a way to an effective interaction between magnetic moments (Si) of the form as depicted in equation (1).

$$H_{DM} = (S_1 \times S_2).D \tag{1}$$

The spin moments induced are function of the vector D. In 3D skyrmion lattice the magnetization distribution in core of skyrmion elucidates chiral amplifications along the 'z' direction of cell axis. DMIs are described by inhomogeneous invariants in the form of spatial variations of the magnetization 'm' with the chiral structures in magnetic materials with DMI the magnetization in spherical coordinates that spatially depend on coordinates as depicted in equation (2).

$$m = (m_x, m_y, m_z) = (\sin\Theta\cos\Psi, \sin\Theta\cos\Psi, \cos\Theta) \tag{2}$$

Where ($\Theta$, $\Psi$) are spherical angles. In the general case, $\Theta$ = $\Theta$(r, $\phi$, z) and $\Psi$ = $\Psi$(r, $\phi$, z) with (r, $\phi$, z) being the cylindrical coordinates. In the case of magnetic configurations without amplification along the thickness of the sample, $\Theta$ and $\Psi$ are specified independent of the z-direction. For a two dimensional case of magnetization profile of the skyrmion the confined geometry spins at the edges of the system vary with little tilt due to the edge condition and, because of confinement, at zero magnetic field the skyrmions can be stabilized [11]. The three skyrmions are equal in energy; the magnetization profile is the function of the accepted solution for the $\Psi$ angle when described in spherical coordinates. The out of plane component of the spins must match for the three skyrmionic configurations [12]. Analytically solving this system, the $\phi$ angle is calculated for the solution of skyrmion with the corresponding boundary condition. To distinguish between the three different systems, the skyrmion radius $r_{sk}$ is computed by finding the value of r where $m_z(r) = 0$, and the radial component of the spins mr located at a distance rsk from the disk centre. Since spins are in-plane at r = $r_{sk}$, then $\Theta = \pi/2$ and the radial component as a function of $\phi$ is as depicted in the equations (3) and (4).

$$m_r(r_{sk}, \Phi) = \sin(\Theta(r_{sk}))\cos(\Psi - \Phi) \tag{3}$$

$$m_r(r_{sk}, \Phi) = \cos(\Psi - \Phi) \tag{4}$$

The comparison of tilting at the system boundary, is improved by a strong DMI, with the semi-analytical solution, the quasi-uniform solution is considered and take advantage of an easy evaluation of $\Theta$ at the edges of the system [13]. The alternative condition for $\Theta$ is as depicted in equation (5).

$$\sin\Theta = \pm\Delta/\zeta \tag{5}$$

The equation (6) depicts a quasi-uniform solution, where at the internal of sample $\Theta$ is constant, equal to zero, and its first derivative. This condition is formulated when the significantly large anisotropy is available in the system. The ratio of vector D and the critical magnitude is depicted by equation (6) as

$$D_c = 4\sqrt{A} * \sqrt{K_u}/\pi \tag{6}$$

The skyrmion radius is explored by considering system parameters for the finite difference simulations and the relevant parameters are considered for Helix period and saturation field as depicted in equations (7) and (8).

$$L_D = 4\pi A/|D| \tag{7}$$

$$H_D = D^2/2 \times A \times M_s \tag{8}$$

Similar to the Bloch like nature, the skyrmions have been found in several metallic cubic B20 compounds and a bulk type Néel texture have been found in two non-metallic oxides [14]. The research is devoted to investigation of Neel skyrmions in an exchange coupled cobalt / palladium multilayers. The first part provides general information about magnetic structure of skyrmions and postulates our achievements. The second part lists the measurement methods and properties of skyrmions. In the third part, the results obtained are presented.

Our Contributions are as follows:

1. By utilizing Lorentz transmission electron microscopy (LTEM) we directly image the skyrmions in thin film multilayer lattice and observe that the dimension of the Néel skyrmions depends on the thickness of the Co/Pd multilayer and repetitively decreases as a monotonically decreasing function with the thickness of the lattice.

2. Utilizing magnetic-imaging and Hall-transport in a functionally viable multilayer sample, the topological-hall resistivity rises over a wide range of temperature and magnetic field with the isolated-skyrmion density is observed.

3. Also it is observed that skyrmions can be stabilized over a wide range of temperature (up-to 220 K).

## 2. Experiment Section

A property of varying skyrmions in exchange coupled cobalt/palladium (co/pd) based multi-layers through current induced spin – orbit torques, can make them extremely exciting and paves a way for future spintronic applications. One of the greatest issues is the need to change the environment of materials in order to create a much broader scope [15]. Here we use D.C magnetron sputtered $[Pt(1nm)/Co(0.5nm)/Pd(1nm)]_{20}$, (the subscript represents the number of repeats) multilayer films where the composition is selected for manifesting skyrmions. The characterization of the films at room temperature specifies DMI, D ≈ 2.0 mJ/m2, and exchange interaction A ≈ 11 pJ/m[8]. The effective magnetic anisotropy (Keff) varies in the range ≈ 0.2 – 0.01 MJ/m$^3$ as temperature (T) is varied from 5 K to 300 K to observe thermodynamically stable skyrmion the field was applied along [0 0 1] direction. The underlying magnetic structure is represented alongside the beam propagation axis by the curl of magnetization [16]. The Néel skyrmion can be observed when the curl of the magnetization lies completely in the plane of the sample. The curl's transformed y-component, which tends to a non-zero z-component when shifted around the x axis, results in formation of Néel skyrmion, with sample tilt of ≈ 30$^o$ for several different temperatures from 200 to 225 K, and thermodynamically stable skyrmions existed from ≈ 210 to ≈ 220 K, and as above 220 K LTEM contrast was not observed. At 200 K there were no skyrmions existed, referring to the non-zero residual beyond-saturation signal. The Fig. 1 illustrates the observation of Néel skyrmions by LTEM. The striped straight blue lines depict the tilt direction, bent arrows represent the rotating direction, and the single skyrmion is marked by blue circle. The $\Delta_{\rho yx}$ varies as a function of $n_{sk}$ for different temperatures (evolution of magnetic textures at T= 5K, 50K, 100K, 150K, 200K, 300K) with the inception of $\Delta_{\rho yx}$ begins at $\mu$0H = 0.3T and further the dashed blue line as seen in the Fig. 1 is a linear fit with slope 0.6 ± 0.1 n. Ω cm/$\mu$m$^2$, and the intercept is calculated as 2.2 ± 0.8 n. $\Omega \cdot cm$.

The temperature dependence is observed between the density of isolated skyrmions ($n_{sk}$), the ordinary hall coefficient ($R_0$), and the approximate estimate for the cumulative error ($\Delta_{\rho yx}$), and the sign of $n_{sk}$ is chosen to match $\Delta_{\rho yx}$. The B20 configurations display a distinctive characteristic slope of straight line ($\Delta_{\rho yx}$) as a function of the magnetic field (H) and temperature (T) applied, corresponding to the skyrmion lattice. The simulated width of the skyrmion

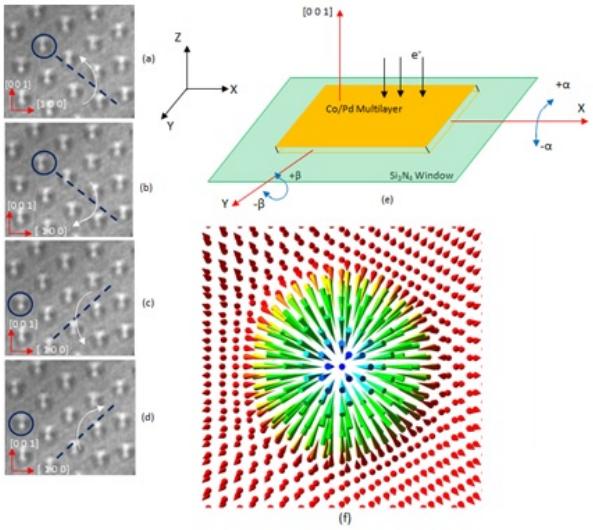


**Fig. 1.** Néel Skyrmion texture evolution as observed in the LTEM (a)-(d) Simulated Lorentz Images (under focused at 1.5 mm recorded at 100 K ) for tilt angle of : (a) $\alpha$ = -8$^o$, (b) $\beta$ = -18$^o$ (c) $\alpha$ = +8$^o$ , (d) $\beta$ = +14$^o$ (e) The $Si_3N_4$ window is 0.5 $\mu$m x 0.5 $\mu$m and 100nm thick and a sample tilting along the x- and y- axis depicting the positive and negative $\alpha$ and $\beta$ tilt angles. (f) Spin texture of Néel Skyrmions.

is observed at different DMI constant (D) values, while varying exchange energy (A) with increasing the exchange energy (A) leads to a larger value of DMI constant (D) necessary to stabilize the skyrmion. The greater DMI constant (D) values contribute to a greater skyrmion size until it exceeds the upper limit and the skyrmion becomes a chiral stripe domain [17]. The value of the skyrmion is estimated a value of the skyrmion as opposed to the experimental width of $|D| = 2.2 \pm 0.3$ mJ.m$^{-2}$, as depicted in Fig. 2(a), this calculated value of 'D' illustrates the existence of zero-field stable skyrmions in multi-layers of Co/Pd, combined with calculations of asymmetric domain wall creep velocities. The Fig. 2(b) illustrates the characteristics plot of domain wall velocity ($\mu$m s$^{-1}$) versus the applied field, here the contributions from DMI is as depicted by the solid lines which represents a modified domain wall creep model [18].

The parameter 'D' is extracted from the velocity curves in Fig. 2(b) and the polarity shift (from – to +) is observed between the repetition number N=2 sample and N=3 sample, further with the increasing repetition number 'N' there is a progressive increase in 'D' as elucidated in Fig. 2(c). This sign change elucidates a large, positive contribution to 'D' from the Co/Pd multilayer structure, and allows further eliminating Pt as the source of the strong positive DMI. For the N = 2 sample, D < 0 is observed, which indicated a huge

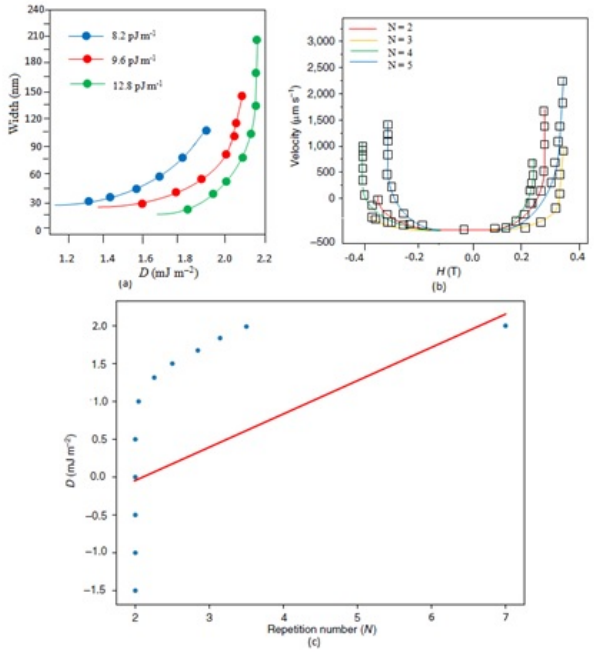


**Fig. 2.** The skyrmion width at different values of D while varying A (b) Domain wall velocity versus applied field (c) The parameter 'D', extracted from the velocity curves in (b).

negative DMI strength for a Pt under layer and for N > 2, with the opposite asymmetry, a large D > 0 is observed. In the B20 systems, the dipole - dipole interactions, which play a prominent role in type-II bubbles and bi-skyrmions, also are found in centrosymmetric systems which are largely proportional to the thickness, can be ignored [19].

## 3. Results Obtained

Bloch skyrmions in chiral B20 systems, where a conflict between Heisenberg exchange and DMI specifies the skyrmion size, demonstrate that the skyrmion size is regardless of material thicknesses [20]. Here the skyrmion radius is denoted as ($r_{sk}$) along with magnetization along 'z' axis $m_z$ ($r_{sk}$) is 0, is at spherical angle of $\Theta = \pi/2$, and the magnetization along $m_x$ is cos Ψ. Now the points where y = 0 , Φ = 0 and $\Psi = \Pi/2+\Psi \sim= \arccos(m_x(r = r_{sk}))$ are considered at the edges ($\Psi \sim= \pi * L/LD$) , and the plot of Néel vectors are obtained as ($m_x$) component and radial component ($m_r$) at the bottom and top of the sample are as depicted in Fig. 3 and Fig. 4 respectively.

The interactions are formulated such as exchange, DMI, and a Uniaxial Anisotropy along 'z' axis. Here the radial profile is computed across co/pd multilayer thickness and with discretization component, a helical spin is observed along the thickness of the co/pd multilayer, which varies

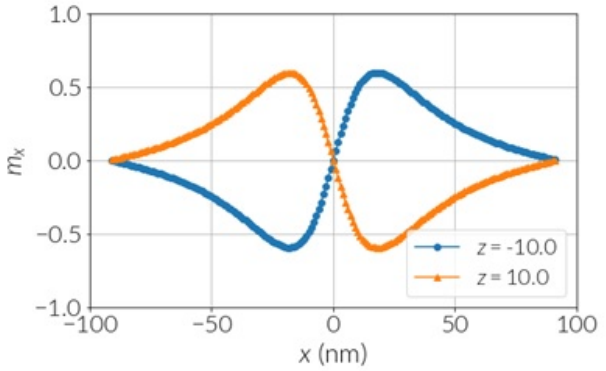


**Fig. 3.** Plot of $m_x$ component at the bottom and top of the sample.

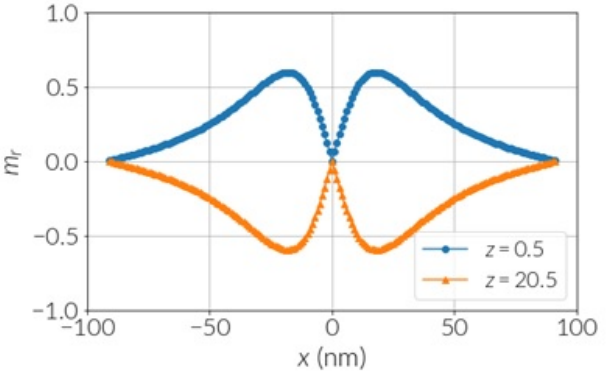


**Fig. 4.** Plot of $m_r$ component at the bottom and top of the sample.

the skyrmionic structure in all layers.

The manifested perpendicular magnetic anisotropy (PMA) in the multilayer film is observed at room temperature with an effective anisotropy of $K_{u,eff}$ = 0.26 $MJm^3$ with anisotropy vector in axis of (0, 0 , 1) and saturation magnetization is $M_s$ = 860 $kAm^{-1}$. The Fig. 5 illustrates vibrating sample magnetometer (VSM) hysteresis measurements of the film developed on thermally oxide Silicon wafer with the observed slope reversal indicating the domain arbitrated reversal. As the sample is tilted, the Néel skyrmions in LTEM is observed and in the applied field, the in-plane component is obtained and the stability of the Néel skyrmions is explored in the presence of an in-plane magnetic field using MFM with fabricating the uniform thin film multilayer square lattice with nearly 900 nm thickness.

The Typical MFM data is presented in Fig. 6 is obtained after cooling from 300 to 100 K in the presence of a magnetic field H(T) = 0.096T, applied perpendicular to the thin film multilayer lattice with a stabilized cycloid intgrated cycloid

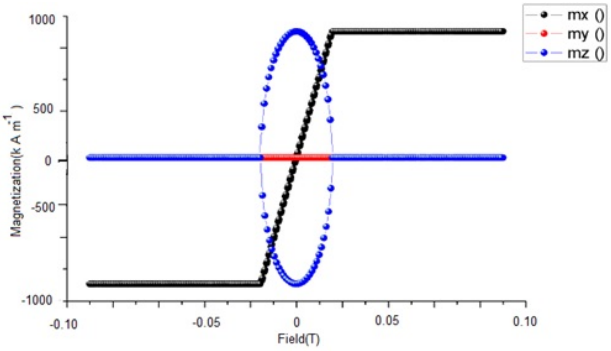


**Fig. 5.** VSM Hysteresis curve.

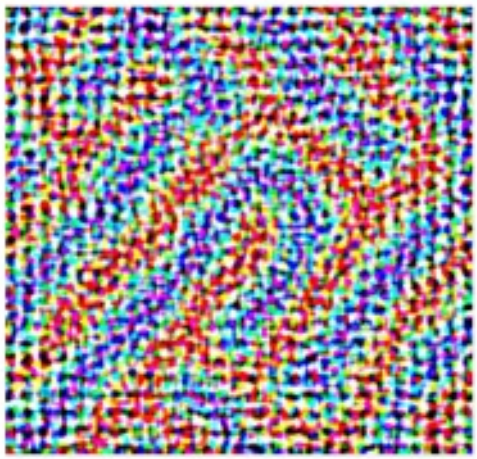

**Fig. 6.** MFM image of Néel skyrmions in 0.096 T at 100 K.

skyrmion phase.

At the start, the skyrmions are stabilized at 100 K after the field cooling process, similar as before and then the out-of-plane field was reduced to zero, next a pure in-plane field was applied, then up to in-plane fields with large strengths of 1 T, the skyrmions are found to be stable as observed Figs. 7(a) and (b) and there is a small decrease in contrast at these high in-plane fields as depicted in Figs. 8 (a) and (b).

## 4. Conclusions

In conclusion, to trace the evolution of nanoscale Ne´el skyrmios in Co/Pd multilayers, the L-TEM is utilized. The existence of zero-field static skyrmions in multilayer Co/Pd, exchange coupled with measurements of asymmetric domain wall creep velocities, has allowed us to estimate D= 2.2 ± 0.3 mJ.m$^{-2}$. Specific multilayers, which have already shown strong spin – orbit - torque (SOT) efficiencies in computer geometries, paves the way for further research with regard to the logic and storage systems based on skyrmion.

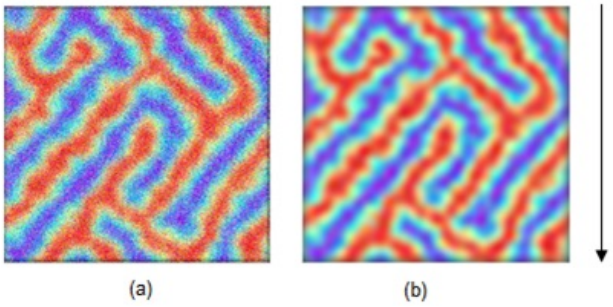


**Fig. 7.** MFM images of meta-stable Néel skyrmions in-plane magnetic field of strength: a) 0T b) 0.3T at 100K.

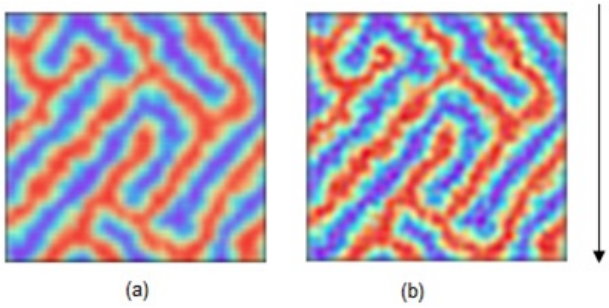


**Fig. 8.** MFM images of meta-stable Néel skyrmions in-plane magnetic field of strength: a) 0.6 T b) 1T at 100K.

## References

[1] Shawn D Pollard, Joseph A Garlow, Jiawei Yu, Zhen Wang, Yimei Zhu, and Hyunsoo Yang. Observation of stable Néel skyrmions in cobalt/palladium multilayers with Lorentz transmission electron microscopy. *Nature communications*, 8(1):1–8, 2017.

[2] J Cui, Y Yao, X Shen, Y G Wang, and R C Yu. Artifacts in magnetic spirals retrieved by transport of intensity equation (TIE). *Journal of Magnetism and Magnetic Materials*, 454:304–313, 2018.

[3] Senfu Zhang, Junwei Zhang, Yan Wen, Eugene M Chudnovsky, and Xixiang Zhang. Determination of chirality and density control of Néel-type skyrmions with in-plane magnetic field. *Communications Physics*, 1(1):1–7, 2018.

[4] K Karube, J S White, N Reynolds, J L Gavilano, H Oike, A Kikkawa, F Kagawa, Y Tokunaga, Henrik M Rønnow, and Y Tokura. Robust metastable skyrmions and their triangular–square lattice structural transition in a high-temperature chiral magnet. *Nature materials*, 15(12):1237–1242, 2016.

[5] Peter Milde, Denny Köhler, Joachim Seidel, L M Eng, Andreas Bauer, Alfonso Chacon, Jonas Kindervater, Sebastian Mühlbauer, Christian Pfleiderer, and Stefan

Buhrandt. Unwinding of a skyrmion lattice by magnetic monopoles. *Science*, 340(6136):1076–1080, 2013.

[6] Markus Hoffmann, Bernd Zimmermann, Gideon P Müller, Daniel Schürhoff, Nikolai S Kiselev, Christof Melcher, and Stefan Blügel. Antiskyrmions stabilized at interfaces by anisotropic Dzyaloshinskii-Moriya interactions. *Nature communications*, 8(1):1–9, 2017.

[7] Kai Litzius, Ivan Lemesh, Benjamin Krüger, Pedram Bassirian, Lucas Caretta, Kornel Richter, Felix Büttner, Koji Sato, Oleg A Tretiakov, and Johannes Förster. Skyrmion Hall effect revealed by direct time-resolved X-ray microscopy. *Nature Physics*, 13(2):170–175, 2017.

[8] Sabpreet Bhatti, Rachid Sbiaa, Atsufumi Hirohata, Hideo Ohno, Shunsuke Fukami, and S N Piramanayagam. Spintronics based random access memory: a review. *Materials Today*, 20(9):530–548, 2017.

[9] Riccardo Tomasello, E Martinez, Roberto Zivieri, Luis Torres, Mario Carpentieri, and Giovanni Finocchio. A strategy for the design of skyrmion racetrack memories. *Scientific reports*, 4:6784, 2014.

[10] P Lai, G P Zhao, H Tang, N Ran, S Q Wu, J Xia, X Zhang, and Y Zhou. An improved racetrack structure for transporting a skyrmion. *Scientific reports*, 7:45330, 2017.

[11] Raí M Menezes, Jeroen Mulkers, Clécio C de Souza Silva, and Milorad V Milošević. Deflection of ferromagnetic and antiferromagnetic skyrmions at heterochiral interfaces. *Physical Review B*, 99(10):104409, 2019.

[12] Kyoung-Whan Kim, Kyoung-Woong Moon, Nico Kerber, Jonas Nothhelfer, and Karin Everschor-Sitte. Asymmetric skyrmion Hall effect in systems with a hybrid Dzyaloshinskii-Moriya interaction. *Physical Review B*, 97(22):224427, 2018.

[13] Riccardo Tomasello, E Martinez, Roberto Zivieri, Luis Torres, Mario Carpentieri, and Giovanni Finocchio. A strategy for the design of skyrmion racetrack memories. *Scientific reports*, 4:6784, 2014.

[14] Ivan Lemesh, Felix Büttner, and Geoffrey S D Beach. Accurate model of the stripe domain phase of perpendicularly magnetized multilayers. *Physical Review B*, 95(17):174423, 2017.

[15] Xichao Zhang, Jing Xia, Yan Zhou, Daowei Wang, Xiaoxi Liu, Weisheng Zhao, and Motohiko Ezawa. Control and manipulation of a magnetic skyrmionium in nanostructures. *Physical Review B*, 94(9):94420, 2016.

[16] Ajaya K Nayak, Vivek Kumar, Tianping Ma, Peter Werner, Eckhard Pippel, Roshnee Sahoo, Franoise Damay, Ulrich K Rößler, Claudia Felser, and Stuart S P Parkin. Magnetic antiskyrmions above room temperature in tetragonal Heusler materials. *Nature*, 548(7669):561–566, 2017.

[17] Ales Hrabec, Joao Sampaio, Mohamed Belmeguenai, Isabell Gross, Raphael Weil, Salim Mourad Chérif, A Stashkevich, Vincent Jacques, Andre Thiaville, and Stanislas Rohart. Current-induced skyrmion generation and dynamics in symmetric bilayers. *Nature communications*, 8(1):1–6, 2017.

[18] Tianli Jin, Durgesh Kumar, Weiliang Gan, Mojtaba Ranjbar, Feilong Luo, Rachid Sbiaa, Xiaoxi Liu, Wen Siang Lew, and S N Piramanayagam. Nanoscale compositional modification in Co/Pd multilayers for controllable domain wall pinning in racetrack memory. *physica status solidi (RRL)–Rapid Research Letters*, 12(10):1800197, 2018.

[19] Albert Fert, Nicolas Reyren, and Vincent Cros. Magnetic skyrmions: advances in physics and potential applications. *Nature Reviews Materials*, 2(7):1–15, 2017.

[20] A Kurenkov, C Zhang, S DuttaGupta, S Fukami, and H Ohno. Device-size dependence of field-free spin-orbit torque induced magnetization switching in antiferromagnet/ferromagnet structures. *Applied Physics Letters*, 110(9):92410, 2017.